Genetic interaction between *hoxb-5* and *hoxb-6* is revealed by nonallelic noncomplementation

Derrick E. Rancourt, Teruhisa Tsuzuki,[1] and Mario R. Capecchi[2]

Howard Hughes Medical Institute, Department of Human Genetics
University of Utah School of Medicine, Salt Lake City, Utah 84112 USA

hoxb-5 **and** ***hoxb-6*** **are adjacent genes in the mouse** ***HoxB*** **locus and are members of the homeotic transcription factor complex that governs establishment of the mammalian body plan. To determine the roles of these genes during development, we generated mice with a targeted disruption in each gene. Three phenotypes affecting brachiocervicothoracic structures were found in the mutant mice. First,** ***hoxb-5***$^{-}$ **homozygotes have a rostral shift of the shoulder girdle, analogous to what is seen in the human Sprengel anomaly. This suggests a role for** ***hoxb-5*** **in specifying the position of limbs along the anteroposterior axis of the vertebrate body. Second,** ***hoxb-6***$^{-}$ **homozygotes frequently have a missing first rib and a bifid second rib. The third phenotype, an anteriorizing homeotic transformation of the cervicothoracic vertebrae from C6 through T1, is common to both** ***hoxb-5***$^{-}$ **and** ***hoxb-6***$^{-}$ **homozygotes. Quite unexpectedly,** ***hoxb-5, hoxb-6*** **transheterozygotes (*hoxb-5*$^{-}$*hoxb-6*$^{+}$*/hoxb-5*$^{+}$ hoxb-6^{-}) also show the third phenotype. By this classical genetic complementation test, these two mutations appear as alleles of the same gene. This phenomenon is termed nonallelic noncomplementation and suggests that these two genes function together to specify this region of the mammalian vertebral column.**

[*Key Words*: Gene targeting; *Hox* genes; nonallelic noncomplementation; cervicothoracic vertebrae; forelimbs; homeotic transformations]

Received October 21, 1994; revised version accepted November 17, 1994.

Genetic analysis of *Drosophila* has revealed a hierarchy of genes that regulate embryonic development. A critical position in this hierarchy is occupied by the homeotic gene complex (*HomC*), which encodes eight transcription factors that share a common DNA-binding motif known as the homeo domain (Kissinger et al. 1990; Otting et al. 1990). In *Drosophila*, these genes act as master switches, governing the formation of parasegmental identity through the activation and/or repression of downstream effector genes (Akam 1987). Mutations in these genes result in changes of parasegmental identity (Lewis 1978).

In mammals, the homeotic complex (*Hox*) is a multigene family composed of 38 genes organized as four linkage groups on four separate chromosomes. These tandem arrays (designated *HoxA*, *HoxB*, *HoxC*, and *HoxD*) bear remarkable structural similarity to *HomC* (Scott 1992). In the mouse, as in *Drosophila*, the chromosomal order of the homeotic genes reflects the relative position of *Hox* gene expression along the anteroposterior (A/P) axis of the developing embryo (Duboule and Dollé 1989; Graham et al. 1989). By analogy, the *Hox* genes are also thought to act as master switches specifying regional information along the A/P axis during mammalian embryogenesis.

Based on DNA sequence similarities, the genes in each *Hox* cluster have been aligned into 13 subfamilies or paralogous groups (Scott 1992). Each paralogous group contains at least two members from separate linkage groups. The *HoxB* locus, which most closely resembles *HomC* organization, has only the first nine paralogous groups. Within the *HoxA*, *HoxC*, and *HoxD* clusters, four more paralogous groups have been described, presumably derived through the duplication of the ancestral *Abd-B* gene (Kappen et al. 1989; Garcia-Fernandez and Holland 1994).

The similarities in both the structure and expression patterns among genes of the same paralogous group have led to the hypothesis that paralogous *Hox* genes perform overlapping functions and that A/P regional identity may be dictated by the combination of *Hox* genes expressed within a given region (Hunt et al. 1991; Holland et al. 1992). Targeted mutations in numerous mouse *Hox* genes have resulted in regionally restricted defects occurring at or near the gene's anterior expression boundary (Chisaka and Capecchi 1991; Lufkin et al.

[1]Present address: Department of Biochemistry, Medical Institute of Bioregulation, Kyushu University, Higashi-Ku, Fukuoka City 812, Japan.
[2]Corresponding author.

Chisaka et al. 1992; LeMouellic et al. 1992; Carpenter et al. 1993; Condie and Capecchi 1993; Mark et al. 1993; Dollé et al. 1993; Gendron-Maguire et al. 1993; Jeannotte et al. 1993; Ramirez-Solis et al. 1993; Rijli et al. 1993; Small and Potter 1993; Condie and Capecchi 1994; Davis and Capecchi 1994; Kostic and Capecchi 1994). In many cases, as seen in *Drosophila*, loss of a specific *Hox* gene results in a respecification of a structure to a more anterior or posterior fate. This has been demonstrated most clearly in mutants that exhibit transformations of the vertebral column.

The role of *Hox* genes in the vertebrate body plan, however, is more complex than in insects, functioning in regions where overt segmentation is not apparent (Dollé et al. 1993; Small and Potter 1993; Davis and Capecchi 1994). Expansion of the homeotic complex in vertebrates, therefore, may have permitted the diversification and specialization of various members of the complex, while at the same time increasing the potential for genetic redundancy. Analysis of the genetic interactions between *Hox* genes has just begun. For example, mice mutant for both *hoxa-3* and *hoxd-3* show that these two paralogous genes interact strongly and quantitatively (Condie and Capecchi 1994). Although mice mutant for the individual genes show no overlap in phenotype (Chisaka and Capecchi 1991; Condie and Capecchi 1993), mice mutant for both genes show a dosage dependent exacerbation of the phenotypes present in each mutant.

Here, we describe the interactions between two adjacent *Hox* genes within the same linkage group. Targeted disruption of *hoxb-5* and *hoxb-6* results in several defects that are confined to the mesodermally derived, brachiocervicothoracic structures. Mice heterozygous for either the *hoxb-5* or *hoxb-6* mutation show no mutant phenotype. Mice homozygous for the *hoxb-5*$^-$ or *hoxb-6*$^-$ disruption each show two phenotypes, one that is unique to the *hoxb-5*$^-$ or *hoxb-6*$^-$ mutation and the other that is observed in both *hoxb-5*$^-$ and *hoxb-6*$^-$ homozygotes. *hoxb-5*$^-$/*hoxb-5*$^-$ mice have an anterior displacement of the shoulder girdle relative to the vertebral column. *hoxb-6*$^-$/*hoxb-6*$^-$ mice display first and second rib defects. Both *hoxb-5*$^-$ and *hoxb-6*$^-$ homozygotes show anteriorizing homeotic transformations of cervicothoracic vertebrae C6 through T1. Surprisingly, transheterozygotes (*hoxb-5*$^-$*hoxb-6*$^+$/*hoxb-5*$^+$*hoxb-6*$^-$) also display the cervicothoracic abnormality. Such nonallelic noncomplementation between these two heterozygous mutations is most readily, though not exclusively, explained if the products of the two genes function as a complex.

Results

Targeted disruption of the hoxb-6 *and* hoxb-5 *genes*

Figure 1A shows the targeting vectors pB6neo2TK and pB5neo2TK that were used to disrupt the *hoxb-6* and *hoxb-5* genes, respectively, via homologous recombination (Capecchi 1989, 1994). pB6neo2TK contains 10.1 kb of mouse genomic DNA encompassing the *hoxb-6* gene, with a *neomycin* resistance (*neo*^{r}) gene derived from pKT3NP4 (Deng et al. 1993) inserted into the coding sequence of the first exon. Similarly, pB5neo2TK contains 8.9 kb of mouse genomic DNA encompassing the *hoxb-5* gene, with the *neo*^{r} gene from pMC1neopA (Thomas and Capecchi 1987) inserted into the coding sequence of the first exon (Krumlauf et al. 1987). Flanking the mouse sequences in both targeting vectors are the thymidine kinase genes (*TK1*, *TK2*) of herpes simplex virus type I and type II (HSV-1 and HSV-2, respectively). Both pB6neo2TK and pB5neo2TK were introduced individually into CC1.2 embryonic stem (ES) cells by electroporation. Cells that had undergone a gene targeting event were enriched by positive–negative selection (Mansour et al. 1988) and identified by Southern blot analysis using flanking hybridization probes. These cell lines were analyzed with additional restriction enzymes and probes to confirm the integrity of the targeted locus on both sides of the *neo* insertion. Representative Southern blots of the DNA from targeted cell lines that were used to generate germ-line chimeras for *hoxb-6* and *hoxb-5* are shown in Figure 1, B and D, respectively. Cells from both clones were injected into C57Bl/6J blastocysts to generate germ-line chimeras.

Mice heterozygous for either the *hoxb-6*$^-$ or *hoxb-5*$^-$ mutations were interbred to generate homozygotes. Southern blots were used to genotype the offspring of the *hoxb-6*$^-$ and *hoxb-5*$^-$ pedigrees, respectively (Fig. 1C,E). Heterozygous intercrosses of either *Hox* gene mutation gave rise to the expected Mendelian genotype ratio at weaning. Mice of both sexes homozygous for either the *hoxb-5* or *hoxb-6* mutation are viable and fertile.

Forelimbs are shifted anteriorly in hoxb-5$^-$ *homozygotes*

hoxb-5$^-$ mutant animals show malformations of both the axial and appendicular skeletons. The forelimbs of *hoxb-5*$^-$ homozygotes are shifted anteriorly relative to the axial skeleton (Fig. 2). This results in a V-shaped shoulder girdle in homozygous mutants (Fig. 2B) compared with heterozygous (Fig. 2A) or wild-type mice (not shown). Occasionally this shift was unilateral (Fig. 2C). Lateral views of these mutant animals demonstrate that the forelimbs are shifted anteriorly by the distance of one and sometimes two cervical vertebrae, with the rostral edge of the scapula aligning with the fourth or third cervical vertebrae instead of the fifth (not shown).

The bones of the shoulder girdle appear normal in *hoxb-5*$^-$ homozygotes, suggesting that this phenotype results from a change in the position of the shoulder relative to the axial skeleton. Such an alteration could occur early in development, when the position of the forelimb is specified, or could be attributable to a later defect in the formation of the musculature. To examine the position of the developing limb in *hoxb-5*$^-$ embryos prior to the elaboration of the musculature, embryonic day 13.5 (E13.5) embryos were eviscerated and stained for both nerve tissue and cartilage. *hoxb-5*$^-$ homozy-

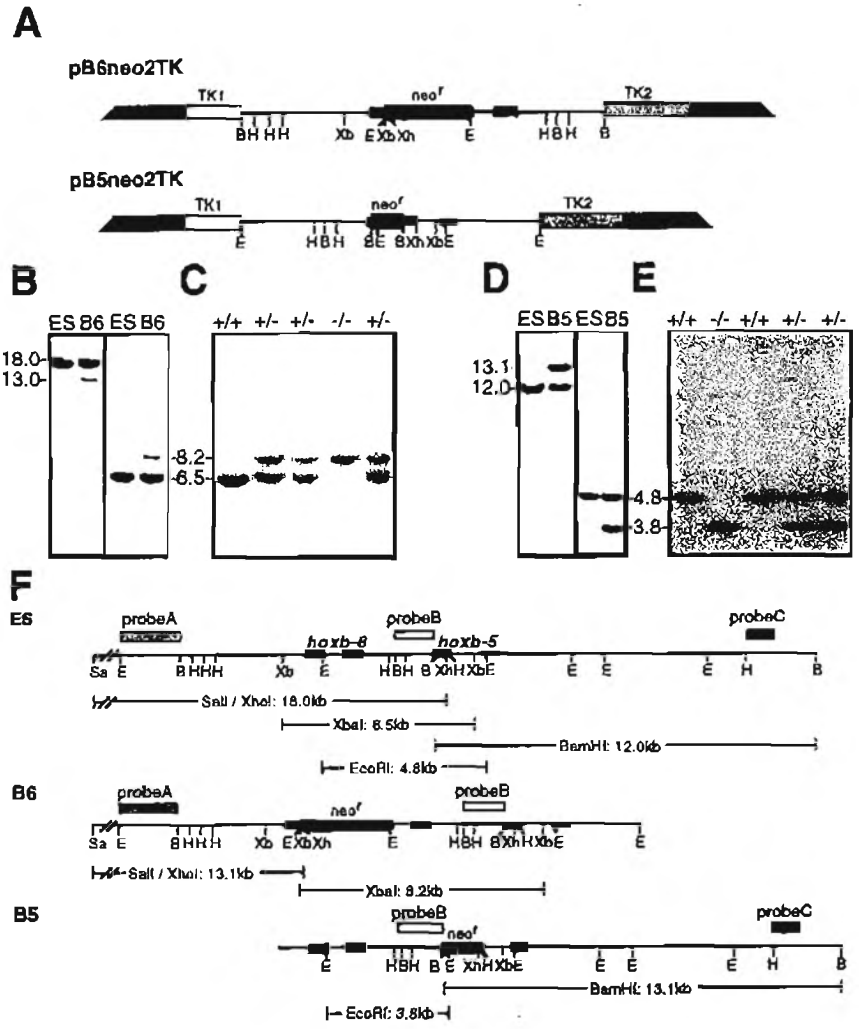

Figure 1. *hoxb-6* and *hoxb-5* targeting and genotypic analysis. (*A*) Structure of the replacement targeting vectors pB6neo2TK and pB5neo2TK. *Eco*RI (E), *Bam*HI (B), *Hin*dIII (H), *Xba*I (Xb), and *Xho*I (Xh) restriction sites within each targeting vector are indicated. First and second exons of each gene are represented by solid boxes. The 5′ → 3′ orientation of the *hoxb-6*, *hoxb-5*, neopA (*neo*^{r}), HSV-1 TK (*TK1*), and HSV-2 TK (*TK2*) genes is *left* to *right*. (*B,D*) Southern blot analysis of *hoxb-6* (*B*) and *hoxb-5* (*D*) targeted ES cells. (*B*) Genomic DNA from the parental cell line, CC1.2 (ES) and the *hoxb-6* targeted cell line (B6), was digested with *Sal*I–*Xho*I (*left*) or *Xba*I (*right*). (*D*) Genomic DNA from the parental cell line, CC1.2 (ES), and the *hoxb-5* targeted cell line (B5), was digested with *Bam*HI (*left*) and *Eco*RI (*right*). The *left* panel *B* was hybridized with a 2.5-kb *Eco*RI–*Bam*HI fragment (Fig. 1F, probe A) lying immediately 5′ to genomic sequences used in the pB6neo2TK targeting vector. The hybridizing fragment that shifts down from 18.0 to 13.0 kb represents the disrupted *hoxb-6*$^-$ allele in cell line 2c6. The *left* panel of *D* was hybridized with a 0.9-kb *Hin*dIII–*Sau*3A fragment (Fig. 1F, probe C) lying 3′ to genomic sequences used in the pB5neo2TK targeting vector. The hybridizing fragment that shifts up from 12.0 to 13.1 kb indicates the disrupted *hoxb-5*$^-$ allele. The *right* panels of both *B* and *D* were hybridized with an internal 1.5-kb *Bam*HI fragment (Fig. 1F, probe B). The hybridizing fragments that shift up from 6.5 to 8.2 kb (*B*) and shift down from 4.8 to 3.8 kb (*D*) represent the *hoxb-6*$^-$ and *hoxb-5*$^-$ alleles, respectively. (*C,E*) Southern blot analysis of genotypes in the *hoxb-6*$^-$ (*C*) and *hoxb-5*$^-$ (*E*) pedigrees. Genomic DNAs prepared from tails of *hoxb-6*$^-$ (*C*) and *hoxb-5*$^-$ (*E*) intercross progeny were digested with *Xba*I and *Eco*RI, respectively, and probed with the internal fragment, probe B. The corresponding genotypes are indicated at the *top* of each gel. (*F*) Diagram of the *hoxb-6–hoxb-5* region in CC1.2 (ES) cells, and in *hoxb-6* (B6) and *hoxb-5* (B5) targeted cells. The bars represent restriction fragments generated from the Southern analysis in *B–E*. Probes used in genomic DNA analysis (probes A, B, and C) are indicated.

gotes with anteriorly shifted forelimbs could be observed as early as day 13.5 of embryogenesis (Fig. 3B). Of 13 homozygous mutant embryos, 10 animals clearly showed that the position of the limbs was shifted relative to the vertebral column, and in all cases but one, the shifts were bilateral. No shifts were observed in 12 heterozygous controls (Fig. 3A). One consequence of the shift is that the brachial plexus enters the forelimb at a more posterior position. This more posterior articulation of the brachial plexus was also observed using a second method to characterize the anterior shift of the developing limb. The nerves of the brachial plexus were labeled by injection of fluorescent carbocyanine dye into the cervical nerves of E12.5 embryos. In *hoxb-5*$^-$ homozygotes, the nerves of the brachial plexus enter the forelimb at a more caudal position than in heterozygous controls (Fig. 3, D and C, respectively), where entry occurs at the midpoint of the limb. The relative trajectories of the nerves are similar in both animals, consistent with the interpretation that the limb bud is shifted rostrally in homozygous mutant embryos. This shift was observed bilaterally in seven of seven homozygotes, whereas no shift was observed in six of six heterozygous controls.

Ribs and intercostal nerves are altered in hoxb-6$^-$ *mutant mice*

Skeletal staining of *hoxb-6*$^-$ homozygous mutant animals revealed both costal malformations and defects of the axial skeleton. Homozygous *hoxb-6*$^-$ mice frequently show first and second rib defects (Figs. 4C and 5B,C; Table 1). The absence or shortening of a first rib in

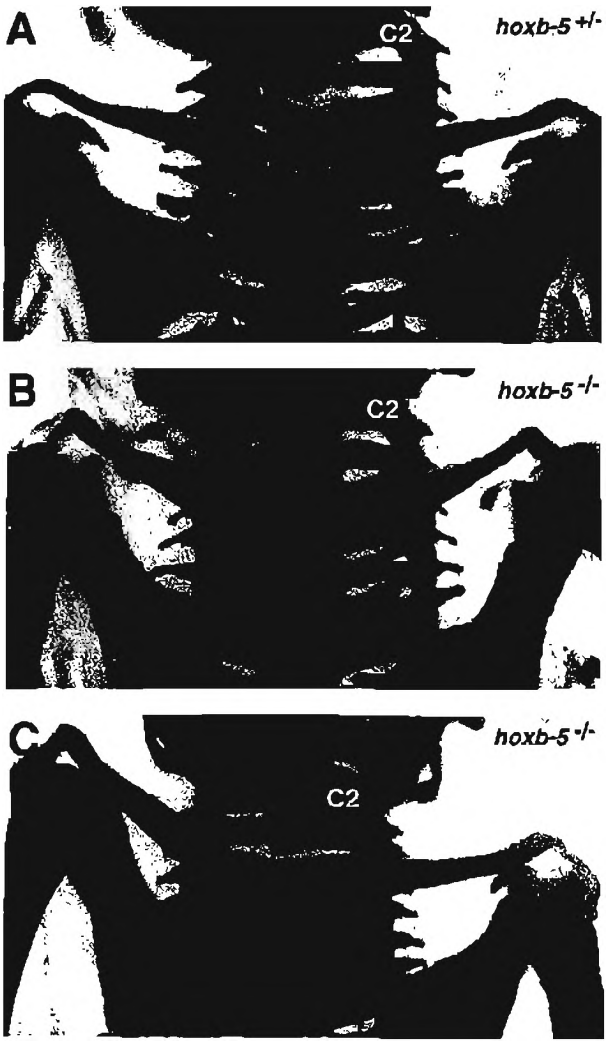

Figure 2. Forelimbs shifted rostrally in *hoxb-5*$^-$ mutant newborns. (*A,B,C*) Ventral views of the lower cervical and upper thoracic regions of a *hoxb-5*$^-$ newborn heterozygote (*A*) and two homozygous mutants (*B,C*). The second cervical vertebra (C2) is indicated. (*B*) A bilateral shift of the forelimbs in this animal results in a V-shaped shoulder girdle. (*C*) A unilateral shift of the left forelimb occurs in this animal.

these animals (Figs. 4C and 5B,E) is coincident with a bifurcation of the second rib such that its upper branch articulates with the top of the sternum. This is unlike the wild-type (Fig. 4A) and heterozygote (not shown) pattern in which the first rib normally articulates with the top of the sternum. It should be noted that when present, this bifurcation occurs consistently at a point that demarcates bone and cartilage in the newborn animal.

The penetrance of this rib phenotype was not complete, occurring in only 50% of the *hoxb-6*$^-$ homozygotes examined. Frequently, true rib defects were restricted to one side, although they were often accompanied by the absence of rib heads on the opposite side of the T1 vertebra (see Fig. 8E, below; Table 1). Although a T2 bifurcation was the predominant rib phenotype seen in *hoxb-6*$^-$ homozygotes, we have observed two variations on the expressivity of this trait. In many cases, it appears that a shortened dorsal first rib successfully articulates with the second rib bifurcation to form an X shape (Fig. 4D; Table 1). In another variation, which we interpret to be more severe, animals either have only a ventral first rib that is attached to the sternum or a gap between the most ventral and dorsal parts of the rib (Fig. 5C; Table 1).

Ribs are formed as ventrolateral projections that emanate from sclerotomes adjacent to the condensing thoracic vertebra and articulate with an independently formed sternum (Chen 1952, 1953). The appearance of both ventral T1 ribs and ventral rib bifurcations in *hoxb-6*$^-$ homozygotes prompted us to investigate rib development in *hoxb-6*$^-$ mutants to determine when the bifurcations occurred. E13.5 embryos were stained for nerve and cartilage at a time prior to the appearance of the sternum. At this stage, embryos with a foreshortened first rib and a bifurcated second rib were clearly seen (Fig. 5B), as were embryos possessing a first rib gap (Fig. 5C).

To examine rib development at earlier stages, E11.5, E12.5, E13.5, and E14.5 embryos were stained in whole mount with the prechondrogenic cell marker peanut agglutinin (Götz et al. 1991). Prechondrogenic rib growth was first detectable in early E11.5 embryos and continued until E13.5 when prechondrogenic sternal rudiments begin to develop in a rostral–caudal direction. A T2 bifurcation was observed in embryos as early as E11.5 (Fig. 5E). The dorsal and ventral aspects of the rib are clearly demarcated at this stage (Fig. 5D,E). Elements proximal to the spinal column are stained only lightly, whereas more lateral elements including the bifurcation are stained more heavily.

Nerve staining in this region also identified alterations in development of the first intercostal nerve in *hoxb-6*$^-$ mutant embryos. Normally this nerve enters in the region between the developing ribs (Fig. 5A). In animals where a bifurcation has occurred, the nerve appears to mimic the bifurcation by crossing medially over to the second intercostal nerve (Fig. 5B). This behavior of the first intercostal nerve is also observed in mutants possessing an X-shaped first and second rib (not shown). Alternatively, in animals where a rib gap has occurred, the nerve does not enter between the first and second rib but, instead, appears to lose its path (Fig. 5C).

Overlapping cervicothoracic transformations in hoxb-6$^-$ *and* hox-5$^-$ *mutant mice*

In addition to the shoulder and rib phenotypes that occur in *hoxb-5*$^-$ and *hoxb-6*$^-$ homozygotes, respectively, a number of overlapping axial transformations are seen in homozygotes from both pedigrees (Figs. 4, 6 and 7; Table 1). Often the tuberculum anterior on the sixth cervical vertebra (C6) either has shifted position to C7 (Figs. 6B,D and 7B,E) or is duplicated on the seventh cervical vertebra (Figs. 4B,C and Fig. 7C). In mutants, a new tuberculum anterior on C7 was accompanied by the appearance

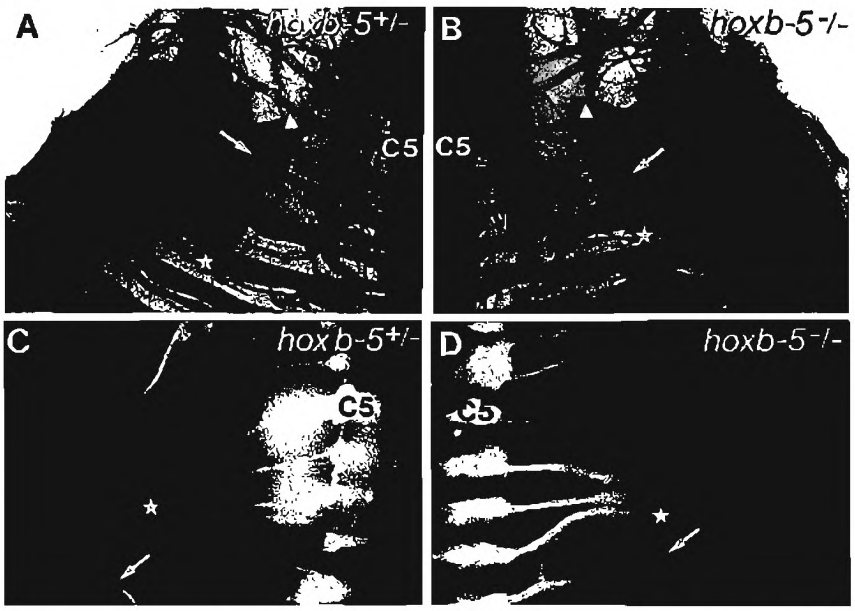

Figure 3. Forelimbs shifted rostrally in *hoxb-5*$^-$ mutant embryos. (*A,B*) Ventral views of the lower cervical and upper thoracic regions of an E13.5 *hoxb-5*$^-$ heterozygote (*A*) and homozygous mutant (*B*) immunostained with anti-neurofilament antibody to reveal neurons and counterstained with alcian blue to reveal cartilage. The fifth cervical vertebra (C5) is indicated. (*B*) In the mutant, the scapula is shifted anteriorly relative to the cervical skeleton. The anterior end of the scapula sits above the fifth cervical vertebra and the fourth cervical nerve (white arrowhead), and the posterior end of the scapula (star) is now at the level of the second rib. In the homozygous mutant, the brachial plexus enters the forelimb more posteriorly (white arrow) by crossing the posterior end of the scapula instead of the middle, as seen in the heterozygote. The black arrow indicates that the rib head is also missing on this side of the animal. (*C,D*) Nerve tracing of the brachial plexus in an E12.5 *hoxb-5*$^-$ heterozygote (*C*) and homozygote (*D*). Cervical ganglia of the plexus were injected alternately with the carbocyanine dyes DiI and DiO. The fifth cervical nerve (C5) is indicated. The relative trajectories of both plexuses are similar. However, the plexus (star) is closer to the posterior edge of the forelimb (arrow) in the mutant (*D*) than in the control (*C*), indicating that the forelimb bud is displaced rostrally in the mutant.

of a transverse foramina (Figs. 6B,D and 7B,C,E). Furthermore, histological analysis of homozygous mutants confirms that when the tuberculum anterior is present on C7, the vertebral artery is rerouted through the ectopic foramen to enter the cervical spinal column at C7 (Fig. 7B,C,E).

A duplication of the tuberculum anterior on C7 was interpreted as being a C7 → C6 anteriorizing transformation, whereas a shift of this structure from C6 to C7 indicated that two anteriorizing transformations had occurred: C6 → C5 and C7 → C6. Similarly, the absence of this structure was considered to occur via a C6 → C5 anteriorizing transformation. A third anteriorizing transformation was revealed by the absence of rib heads, the caput costae, on the first thoracic vertebra (T1) (Figs. 3B, 5B,C, 6C,D, and 7D,E). Analysis of T1 vertebrae from adult skeleton preparations demonstrated that those vertebrae that lacked rib heads had altered lateral processes, making them indistinguishable from C7 (Fig. 8D). These vertebrae were interpreted as having undergone a partial T1 → C7 transformation. Although the absence of rib heads always accompanied a T1 → C7 transformation, the reverse was not found to be true: In adult homozygotes, some T1 vertebrae had normal rib head structures with altered lateral processes resembling those of C7 (Fig. 8C).

Variability in the expressivity of these cervicothoracic phenotypes is seen in homozygotes from both pedigrees (Table 1). Frequently, defects are restricted to or are more severe on one side of the animal than on the other (Fig. 6D). Sometimes only a subset of these transformations will appear (Fig. 6B,C). Although for both pedigrees, the T1 → C7 transformation is most predominant, the frequency with which the C6 → C5 and/or C7 → C6 transformations either coappear with T1 → C7 or appear alone is greater in *hoxb-5*$^-$ homozygotes. In *hoxb-6*$^-$ homozygotes the C6 → C5 and/or C7 → C6 transformations only occurred in combination with T1 → C7. In addition, unlike the case of *hoxb-6*$^-$ homozygotes in which the T1 → C7 transformation often coappeared with defects of the rib, no true rib defects were observed in the *hoxb-5*$^-$ pedigree.

A progression in the stages of the T1 → C7 transformation appears to occur in the *hoxb-5*$^-$ and *hoxb-6*$^-$ animals (Fig. 8). In the first stage, which is frequently observed in *hoxb-5*$^-$ homozygotes and to a lesser degree in *hoxb-6*$^-$ homozygotes, the T1 lateral processes resemble those of C7, although both ribs and rib heads remain associated with the T1 vertebra (Fig. 8C). In the second stage, which occurs to the same extent in homozygotes from both pedigrees, one or both rib heads are missing from a T1 vertebra that resembles C7 (Fig. 8D). Finally, as is seen in only the *hoxb-6*$^-$ homozygotes, the rib itself will be missing, resulting in a complete T1 → C7 transformation (Fig. 8E). Thus far, we have only observed T1 vertebrae where one rib is missing, although frequently the opposite rib head will be absent (Fig. 8E; Table 1).

We find that the lateral processes of C7 and T1 are only distinguishable in preparations of adult vertebrae. As a result, it is likely that the number of partial T1 → C7 transformations scored from newborn skeletal preparations is greater than that represented in Table 1. In adult skeletal preparations of both *hoxb-5*$^-$ and

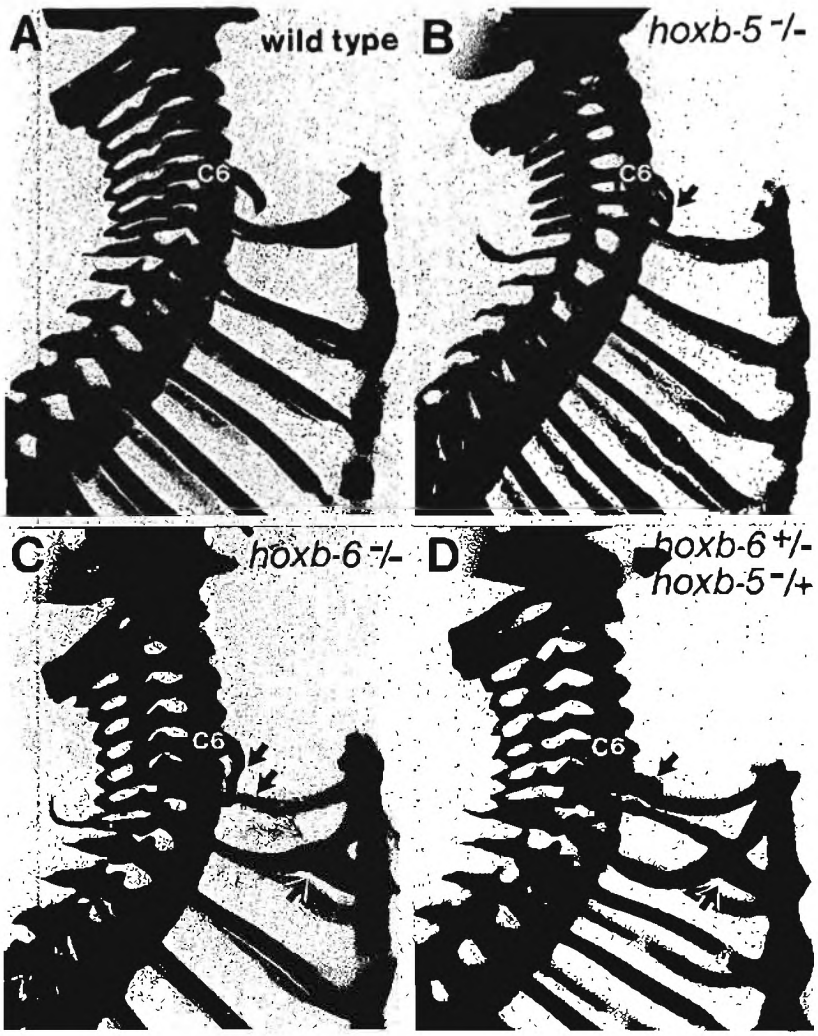

Figure 4. Alterations of the cervicothoracic skeleton in *hoxb-5*$^-$ and *hoxb-6*$^-$ mutants and transheterozygotes. Lateral views of newborn skeleton preparations of wild type (*A*), *hoxb-5*$^-$ homozygote (*B*), *hoxb-6*$^-$ homozygote (*C*), and *hoxb-5*$^-$/*hoxb-6*$^-$ transheterozygote (*D*) are represented. The sixth cervical vertebra (C6) is indicated. (*B*) The arrow points to the fused, duplicated tuberculum anterior present on the seventh cervical vertebra. (*C*) The *top* arrow points to a tuberculum anterior that is altered in this animal. In addition, the first rib is absent on the right side (*middle* arrow) and a bifid second rib occurs (*bottom* arrow). (*D*) The tuberculum anterior shifts from C6 to C7 on both sides of this animal (*top* arrow). The first and second ribs are also bifid (*bottom* arrow) and come together to form an X on the right side of this animal.

hoxb-6$^-$ homozygotes, (18, and 8, respectively), all animals display alterations of their T1 lateral processes, even when no other cervicothoracic phenotypes are apparent. Therefore, it is likely that the penetrance of cervicothoracic phenotypes is higher than indicated in Table 1.

Cervicothoracic phenotypes in hoxb-5$^-$/hoxb-6$^-$ *transheterozygotes*

Because of the considerable overlap in cervicothoracic phenotypes observed in both the *hoxb-5*$^-$ and *hoxb-6*$^-$ pedigrees, we considered the hypothesis that *hoxb-5* and *hoxb-6* may act in concert to specify the development of the lower cervical–upper thoracic region of the animal. Despite the fact that both the *hoxb-5*$^-$ and *hoxb-6*$^-$ mutations gave rise to truly recessive phenotypes, interactions between *hoxb-5* and *hoxb-6* might be revealed in transheterozygotes (i.e., *hoxb-5*$^-$, *hoxb-6*$^+$/*hoxb-5*$^+$ *hoxb-6*$^-$ mice).

In the initial experiments, *hoxb-5*$^-$ and *hoxb-6*$^-$ homozygotes were crossed to generate two litters of transheterozygotes. Of 11 newborn progeny, 8 animals showed cervicothoracic phenotypes typical of homozygotes from either pedigree. One animal possessed bilateral transformations of C6, C7, and T1 as well as an X-shaped first and second rib (Fig. 4D).

To confirm these results, as well as to generate heterozygous control littermates in the same litter, *hoxb-6*$^{-/-}$×*hoxb-5*$^{+/-}$ and *hoxb-5*$^{-/-}$×*hoxb-6*$^{+/-}$ crosses were initiated. Both crosses gave rise to litters where approximately half of the offspring were transheterozygotes and half were control heterozygotes.

Both types of crosses resulted in transheterozygotes bearing cervicothoracic phenotypes (Table 1), whereas no phenotypes were observed in control animals heterozygous for one or the other mutation (not shown). Of sixteen transheterozygotes derived from the first cross, 12 showed cervicothoracic phenotypes, including one with a rib bifurcation. Similarly, the second cross produced 10 of 13 transheterozygotes with cervicothoracic phenotypes. As was seen for both the *hoxb-5*$^-$ and *hoxb-*

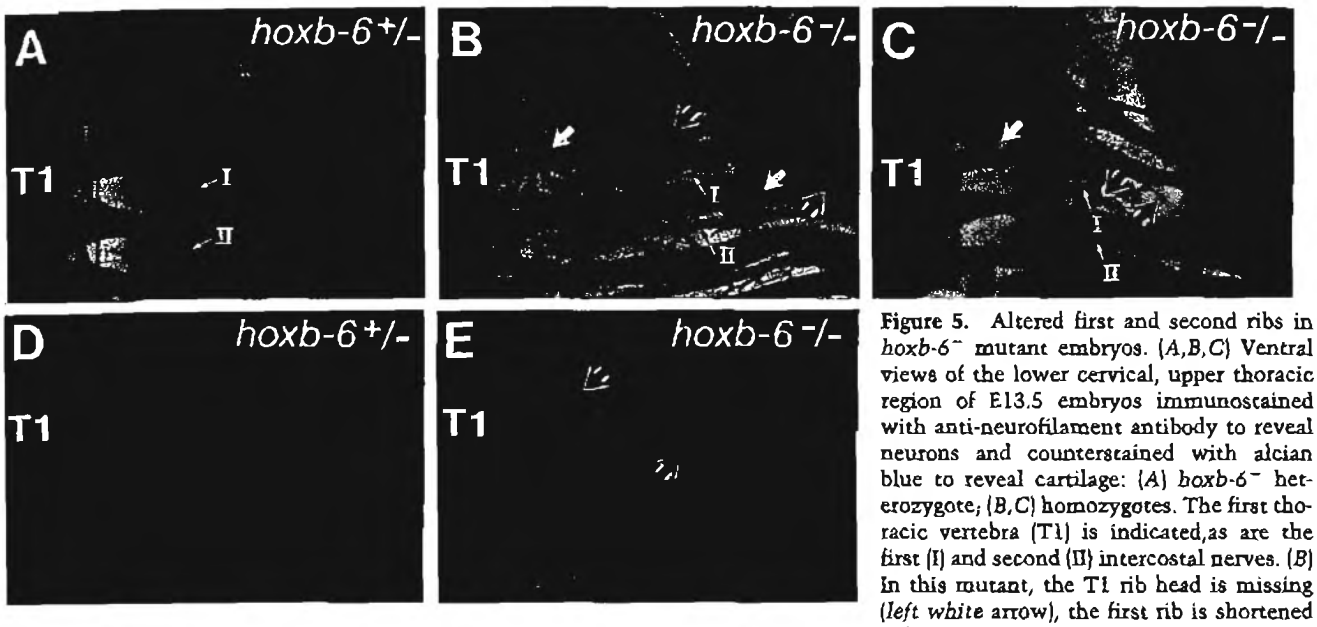

Figure 5. Altered first and second ribs in *hoxb-6*$^-$ mutant embryos. (*A,B,C*) Ventral views of the lower cervical, upper thoracic region of E13.5 embryos immunostained with anti-neurofilament antibody to reveal neurons and counterstained with alcian blue to reveal cartilage: (*A*) *hoxb-6*$^-$ heterozygote; (*B,C*) homozygotes. The first thoracic vertebra (T1) is indicated,as are the first (I) and second (II) intercostal nerves. (*B*) In this mutant, the T1 rib head is missing (*left white* arrow), the first rib is shortened (*left black* arrow), the second rib is bifurcated (*right black* arrow), and the trajectory of the first intercostal nerve is altered such that it crosses over to the second intercostal nerve (*right white* arrow). (*C*) In this mutant the T1 rib head is absent (*left white* arrow), a gap appears in the T1 rib (*right black* arrow) and the first intercostal nerve does not develop (*left black* arrow). (*D,E*) Ventral views of the lower cervical, upper thoracic regions of E11.5 embryos stained with HRP-conjugated peanut agglutinin (PAG). Rib bifurcation is observed in precartilagenous rib blastema: (*D*) *hoxb-6*$^-$ heterozygote; (*E*) homozygote. (*D*) Dorsal and ventral aspects of the rib can be distinguished by the difference in the intensity of PAG staining. Ventral portions of the rib stain more intensely at this stage. (*E*) Bifurcation of the second rib is observed in early rib blastema at the border between the dorsal and ventral aspects of the rib (*bottom* arrow). A shortened first rib also occurs in this embryo (*top* arrow).

6$^-$ homozygotes, the penetrance and expressivity of these traits were variable. However, the variability of this phenotype in transheterozygotes appears to be similar to that observed in *hoxb-5*$^-$ and *hoxb-6*$^-$ homozygotes. For instance, the frequency of C6 → C5 and/or C7 → C6 transformations in transheterozygotes is 52%, whereas in *hoxb-5*$^-$ and in *hoxb-6*$^-$ homozygotes, it is 57 and 36% respectively. In the *hoxb-6*$^-$ homozygotes these transformations only occur in conjunction with a T1 → C7 transformation, whereas for both *hoxb-5*$^-$ homozygotes and transheterozygotes these transformations can appear on their own.

hoxb-6 *and* hoxb-5 *expression is unaltered in* hoxb-5$^-$ *and* hoxb-6$^-$ *mutants, respectively*

Because the *hoxb-5* and *hoxb-6* mutant chromosomes failed to complement each other with respect to the cervicothoracic phenotype, it was important to determine whether *hoxb-5* or *hoxb-6* gene expression was perturbed. Alteration in the expression of one gene in the mutant background of the other could explain why overlapping cervicothoracic phenotypes arise in the two mutants. In wild-type E12.5 embryos, both *hoxb-6* and *hoxb-5* are expressed in the spinal cord to the level of the posterior myelencephalon. In the vertebral column, *hoxb-6* has been reported to be expressed to the level of prevertebra (pv) 8, while the expression of *hoxb-5* extends to pv2 (Graham et al. 1989; Gunt et al. 1990).

The expression patterns of *hoxb-6* and *hoxb-5* in *hoxb-5*$^-$ and *hoxb-6*$^-$ homozygotes, respectively, did not differ from the wild-type patterns (Fig. 9). Using a *hoxb-6* specific RNA probe, we found that expression of *hoxb-6* within the vertebral column extended rostrally to the level of pv8 in both wild-type and *hoxb-5*$^-$ homozygous embryos (Fig. 9A–D). *hoxb-5* expression was monitored both with a specific RNA probe and with an antibody directed against hoxb-5 protein (Wall et al. 1992). Wild-type and *hoxb-6*$^-$ mutant embryos immunostained for hoxb-5 protein were counterstained with alcian blue to localize expression to the prevertebrae. No differences in the expression pattern of hoxb-5 protein or RNA were apparent in wild-type and *hoxb-6*$^-$ homozygous embryos. Rostrally, both RNA and protein extended to pv2. However, although hoxb-5 protein expression was found to extend caudally to only pv8 in both wild-type and *hoxb-6*$^-$ homozygotes (Fig. 9E,F), RNA expression was observed to extend caudally far beyond that point (Fig. 9G,H; Holland and Hogan 1988; Gaunt et al. 1990), implying that *hoxb-5* is regulated post-transcriptionally.

Discussion

We have used targeted gene disruption to assess the roles of *hoxb-5* and *hoxb-6* during murine development. A *neo*–poly(A) cassette was inserted into first exon coding sequences of *hoxb-5* and *hoxb-6*, respectively. This insertion not only disrupts the reading frame of the target

Table 1. *Cervicothoracic phenotypes in newborn hoxb-5⁻, hoxb-6⁻ homozygotes and transheterozygotes*

Genotype	C6 → C5	C7 → C6	T1 → C7	Ribs	C6 → C5 C7 → C6	C6 → C5 T1 → C7	C6 → C5 ribs	C7 → C6 T1 → C7	C7 → C6 ribs	C6 → C5 C7 → C6 T1 → C7	C6 → C5 C7 → C6 ribs
hoxb-6$^{-/-}$			3	5	[a] [c] [a,d] [b,d]		[a] [a,d] [a,c,d]	[g]	[a]	1 [d]	[c,d] [c,f]
hoxb-5$^{-/-}$	1	2	8	1		1 2		3 [g] [d]		4 [h] 2[d] 1[i]	
hoxb-5$^{-/+}$ *hoxb-6*$^{+/-}$		1	7	2		1 [h] 1	1	3		3[d] 2 [k]	2 2[i] [a,d] [a,j] [c,j]

Newborns from *hoxb-6*$^{-}$ and *hoxb-5*$^{-}$ intercrosses (homozygous by heterozygous) and *hoxb-6*$^{-}$ × *hoxb-5*$^{-}$ outcrosses (*hoxb-5*$^{-/-}$ × *hoxb-6*$^{+/-}$, *hoxb-6*$^{-/-}$ × *hoxb-5*$^{+/-}$, *hoxb-5*$^{-/-}$ × *hoxb-6*$^{+/-}$) were analyzed for skeletal defects. Heterozygotes derived from both intercrosses (*hoxb-6*$^{-}$: 28/53; *hoxb-5*$^{-}$: 36/72) and outcrosses (*hoxb-6*$^{-/-}$ × *hoxb-5*$^{+/-}$: 13/29; *hoxb-5*$^{-/-}$ × *hoxb-6*$^{+/-}$: 13/26) showed no skeletal defects. The array of cervicothoracic phenotypes observed in homozygotes and transheterozygotes is listed. A C6 → C5 transformation results in the loss of a tuberculum anterior from the sixth cervical vertebra. In a C7 → C6 transformation, a tuberculum anterior and a vertebral foramen appear on the seventh cervical vertebra. A T1 → C7 transformation is manifest by the absence of a rib head on the first thoracic vertebra. Ribs refer to changes in the structure of the first and/or second rib. The T1 rib head is invariably absent from the side(s) showing a rib defect. Animals that displayed unilateral or bilateral phenotypes are listed on the *left* or *right* side of each category column, respectively. 3/25 *hoxb-6*$^{-}$ homozygotes, 6/35 *hoxb-5*$^{-}$ homozygotes, and 10/40 transheterozygotes showed no phenotype. The phenotypes observed in transheterozygotes do not appear to be influenced by the sex of the mice donating the *hoxb-5*$^{-}$ or *hoxb-6*$^{-}$ mutant alleles; therefore, imprinting of this locus does not appear to be a factor in controlling the activities of these genes.

[a]T1 rib shortened or missing and T2 bifurcation.
[b]Ventral T1 rib only.
[c]T1 and T2 ribs form an X.
[d]T1 → C7 is bilateral.
[e]Gap between dorsal and ventral T1 rib.
[f]Bilateral rib defect.
[g]Unilateral transformations occur on opposite sides.
[h]C6 → C5 is unilateral.
[i]T1 → C7 is unilateral.
[j]Unilateral rib defects occur.
[k]C7 → C6 is bilateral.

gene but also results in premature termination of the native transcript due to the presence of an effective poly(A) addition signal (Condie and Capecchi 1993; Mansour et al. 1993; Kostic and Capecchi 1994).

In situ expression studies have localized *hoxb-5* mRNA and protein to both neuroectodermal and mesodermal lineages in the developing mouse embryo (Holland and Hogan 1988; Kuritani and Wall 1992; Wall et al. 1992). Migrating neural crest cells, which express *hoxb-5*, are thought to contribute to the formation of the nodose ganglion as well as to epibranchial derivatives of the fourth and sixth pharyngeal arches. Histological analysis of *hoxb-5*$^{-}$ homozygotes reveals no defects in the structure of the vagus nerve or any other structures in the circumpharyngeal area. As well, there are no defects in the lungs, gastrointestinal tract or kidneys, all of which express *hoxb-5* during organogenesis. Similarly, no defects are observed in the ventrolateral region of *hoxb-6*$^{-}$ mutant mice, including kidneys, forelimbs and hindlimbs, all of which express *hoxb-6* (Shen et al. 1991; Shughart et al. 1991; Eid et al. 1993). The absence of mutant phenotypes in these tissues, particularly during organogenesis, might derive from functional redundancies among *Hox* genes. Multiple *Hox* genes are expressed in the anlage of tissues giving rise to the lungs, heart, kidneys, gastrointestinal tract, and reproductive organs. The role of *Hox* genes in the formation of these organs may become evident only in mice containing multiple *Hox* gene mutations.

Instead, defects in *hoxb-5*$^{-}$ and *hoxb-6*$^{-}$ mutant mice are restricted to three classes. Two of the classes, defects in the position of the forelimbs and defects in the formation of the first two ribs, are unique to homozygous mutants of *hoxb-5*$^{-}$ and *hoxb-6*$^{-}$, respectively. The third class, which appears in both homozygous mutants, is an anteriorizing homeotic transformation of cervicothoracic vertebrae C6 through T1.

Surprisingly, although the C6 → T1 homeotic transformations are never observed in mice heterozygous for either the *hoxb-5*$^{-}$ or *hoxb-6*$^{-}$ mutation, they do appear in *hoxb-5, hoxb-6* transheterozygotes. Thus, by this genetic complementation criterion, these two individual mutations in separate genes behave as alleles of the same gene. This phenomenon of nonallelic noncomplementation has been described in yeast, *Caenorhabditis elegans*, and *Drosophila* (Rine and Herskowitz 1987; Stearns and Botstein 1988; Hays et al. 1989; Heitman et al. 1991; Varkey et al. 1993 and references therein) and

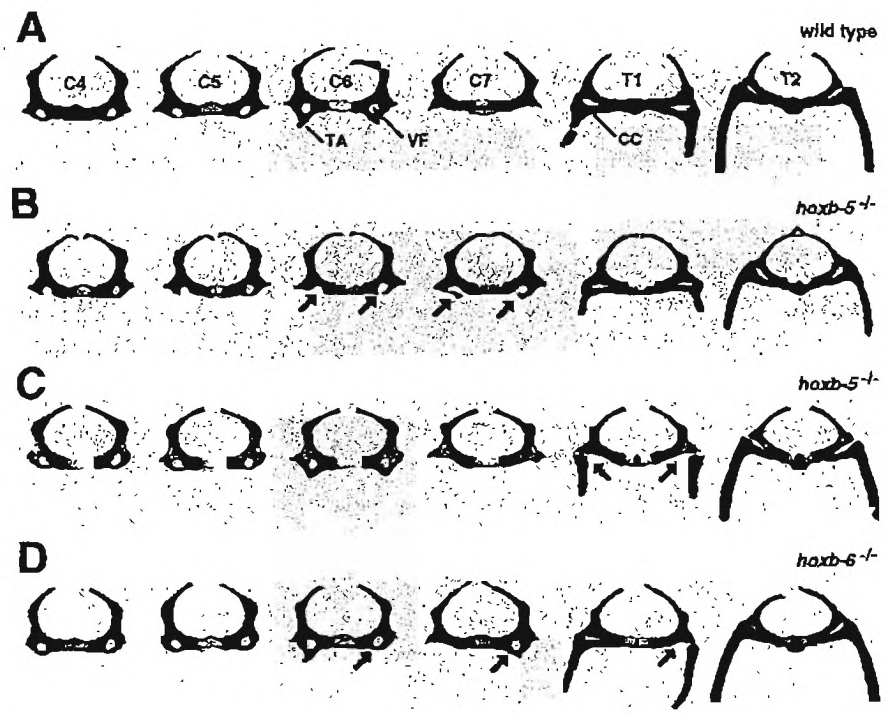

Figure 6. Variable expressivity of cervicothoracic transformations in *hoxb-5*$^-$ and *hoxb-6*$^-$ homozygous newborns. Panels represent rostral views of cervical and thoracic vertebrae in one wild-type (*A*), two *hoxb-5*$^-$ (*B,C*), and one *hoxb-6*$^-$ homozygote (*D*). Ribs were cut free of the sternum. (*A*) The fourth cervical (C4) through to the second thoracic (T2) vertebrae are indicated, as are a tuberculum anterior (TA), vertebral foramen (VF), and rib head (or caput costae, CC). (*B*) Two of three cervicothoracic transformations occur. The tuberculae anterior are absent from C6 and shifted to C7, also resulting in new vertebral foramina on C7 (indicated by arrows). (*C*) The third vertebral transformation represented in this animal shows the absence of rib heads (arrows), resulting in a T1 vertebra that resembles C7 vertebrae with cervical ribs. (*D*) All three cervicothoracic transformations occur on one side of this animal (indicated by arrows).

has often been found to involve disruption of a functional complex formed between the affected gene products.

A model to explain how the *hoxb-5* and *hoxb-6* mutations result both in unique phenotypic consequences and in a common phenotype that displays nonallelic noncomplementation is that these gene products function as homodimers and as heterodimers with the common phenotype, for example, being mediated by the heterodimer. In mice heterozygous for either the *hoxb-5*$^-$ or *hoxb-6*$^-$ mutation, the concentration of the homodimer and of the heterodimer would be one-half of that present in the wild type. Because such mice show no apparent phenotype, this level of gene product is presumed to be sufficient for normal development. However, in transheterozygotes, the amount of heterodimer would be reduced to one-fourth the normal level. This level of gene product is postulated to be below the threshold required for normal development of the cervicothoracic region. Consistent with such a model, studies involving transfection of cultured mammalian cells, as well as biochemical studies, suggest that protein–protein complexes can form between separate *Hox* gene products (Zappavigna et al. 1994).

However, we favor interpreting the nonallelic noncomplementation observed in *hoxb-5*$^-$, *hoxb-6*$^-$ transheterozygotes in terms of the amount of gene product required to mediate a function. For the phenotype held in common, *hoxb-5* and *hoxb-6* would be postulated to perform near identical roles. In normal animals the amount of gene product for this function would then be 4×. In mice heterozygous for either the *hoxb-5*$^-$ or *hoxb-6*$^-$ mutation, the amount of gene product would be 3× and would be sufficient to permit proper development of these vertebrae. However, in transheterozygotes or in mice homozygous for either the *hoxb-5*$^-$ or the *hoxb-6*$^-$ mutation, the level of gene product would be 2× and would not be sufficient for normal development of this region. Furthermore, the similar extent of variability in the penetrance and expressivity of this phenotype in *hoxb-5*$^-$ homozygotes, in *hoxb-6*$^-$ homozygotes, and in *hoxb-5*$^-$, *hoxb-6*$^-$ transheterozygotes could be explained by the presence of the 2× amount of gene product in these mice. Irrespective of the model, observing nonallelic noncomplementation between *hoxb-5*$^-$ and *hoxb-6*$^-$ transheterozygotes indicates that these genes interact to properly specify the identity of the C6 to T1 vertebrae.

The limb phenotype in hoxb-5$^-$ *mutant mice*

Frequently in *hoxb-5*$^-$ homozygotes the position of the shoulder girdle is shifted anteriorly by one or two cervical vertebrae. Because the clavicle bones of the shoulder apparatus are anchored to the top of the sternum, this defect results in a pronounced V-shaped shoulder girdle. The shifting of the limb bud is apparent as early as E12.5, prior to the elaboration of the mouse musculature. In vertebrates, the limb develops as a bud of mesenchymal cells originating from the adjacent lateral plate mesoderm (Chavellier et al. 1977). In mice, *hoxb-5* is expressed in the anteroproximal region of the early forelimb bud (Wall et al. 1992). This expression may occur de novo in the limb bud or it may result from cells that have migrated from the adjacent mesoderm that expresses *hoxb-5* at an earlier stage. The above observations suggest that *Hox* genes not only govern the formation of the

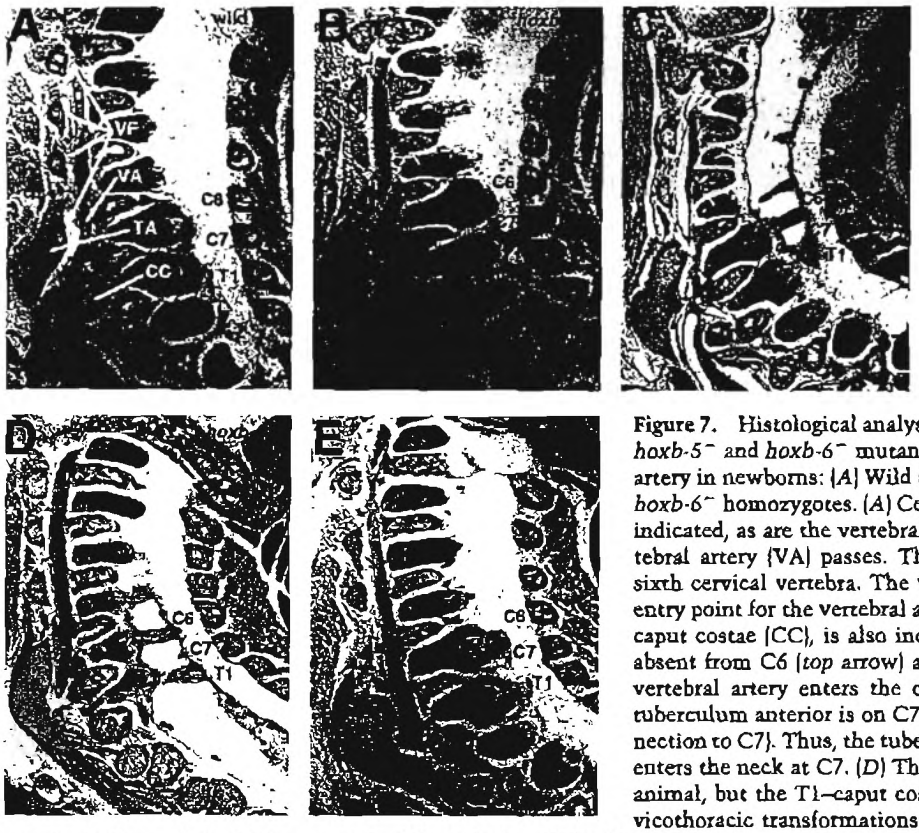

Figure 7. Histological analysis of cervicothoracic transformations in *hoxb-5*$^-$ and *hoxb-6*$^-$ mutants. Parasagittal sections of the vertebral artery in newborns: (*A*) Wild type; (*B,C*) *hoxb-5*$^-$ homozygotes; (*D,E*) *hoxb-6*$^-$ homozygotes. (*A*) Cervicothoracic vertebrae (C6, C7, T1) are indicated, as are the vertebral foramina (VF), through which the vertebral artery (VA) passes. The tuberculum anterior (TA) is on the sixth cervical vertebra. The vertebral foramen on C6 is the normal entry point for the vertebral artery into the neck. The T1 rib head, or caput costae (CC), is also indicated. (*B*) The tuberculum anterior is absent from C6 (*top* arrow) and appears on C7 (*bottom* arrow). The vertebral artery enters the cervical spinal column at C7. (*C*) The tuberculum anterior is on C7 in addition to C6 (arrow indicates connection to C7). Thus, the tuberculae are fused and the vertebral artery enters the neck at C7. (*D*) The tuberculum anterior is normal in this animal, but the T1–caput costae is absent (arrow). (*E*) All three cervicothoracic transformations occur in this animal. The tuberculum anterior is absent from C6 (*top* arrow) and is shifted to C7 (*middle* arrow), where the vertebral artery enters the neck. In addition, the T1–caput costae is absent (*bottom* arrow).

bones in the limb (Dollé et al. 1993; Small and Potter 1993; Davis and Capecchi 1994) but also the positioning of the limbs relative to the axial skeleton, perhaps by providing positional cues to the mesoderm that will give rise to the limb bud. It is curious that in *hoxb-5*$^-$ homozygotes, the shift in the position of the limb bud relative to the axial skeleton and the change in the identity of the cervicothoracic vertebra show opposite directionality. It is as if specification of the position of the forelimb is independent of the identity of the axial skeleton.

The costal phenotype in hoxb-6$^-$ *mutant mice*

Many *hoxb-6*$^-$ mutants have alterations in the development of the first and second ribs. In cases where the dorsal portion of the first rib is absent or shortened, a ventral bifurcation of the second rib is observed, which articulates with the sternum at the level of the first rib. This phenotype is invariably unilateral and results in a thoracic hemivertebra bearing the likeness of the seventh cervical vertebra. The bifurcation of the second rib is evident as early as E11.5, suggesting that the dorsal and ventral aspects of the rib are specified early in costal development. Formation of ventral ribs may involve sensing the presence of the adjacent rostral rib because in its absence a new ventral branch is elaborated. In *hoxb-6*$^-$ mutants that display first and second rib defects, the development of the first intercostal nerve is also altered (Fig. 5B,C), suggesting that communication is an important component of costal development of both bone and nerve. Furthermore, it has been suggested that costal derivatives of the sclerotome and myotome also communicate because disruption of the myotome-specific gene *myf-5* results in rib defects (Braun et al. 1992).

Cervicothoracic homeotic transformations

In *hoxb-5*$^-$ and *hoxb-6*$^-$ homozygotes, we observe overlapping anteriorizing transformations of the cervicothoracic vertebrae C6, C7, and T1. In both mutants, the C6 → C5 transformation is frequently accompanied by a C7 → C6 transformation; together these are manifest by displacement of the tuberculum anterior from C6 to C7. This shift also results in the appearance of a transverse foramen on C7 and entry of the vertebral artery into the neck at C7, rather than C6 (Figs. 6B,D and 7B,E). In newborns, the T1 → C7 transformation is manifest by the absence of rib heads (caput costae) from the first thoracic vertebra, such that T1 resembles a C7 vertebra with cervical ribs (Figs. 6C,D and 7D). In homozygous adults, we observe that the lateral processes of these T1 vertebrae are indistinguishable from those of C7 (Fig. 8). Because these T1 vertebrae have ribs associated with them, this transformation is not complete.

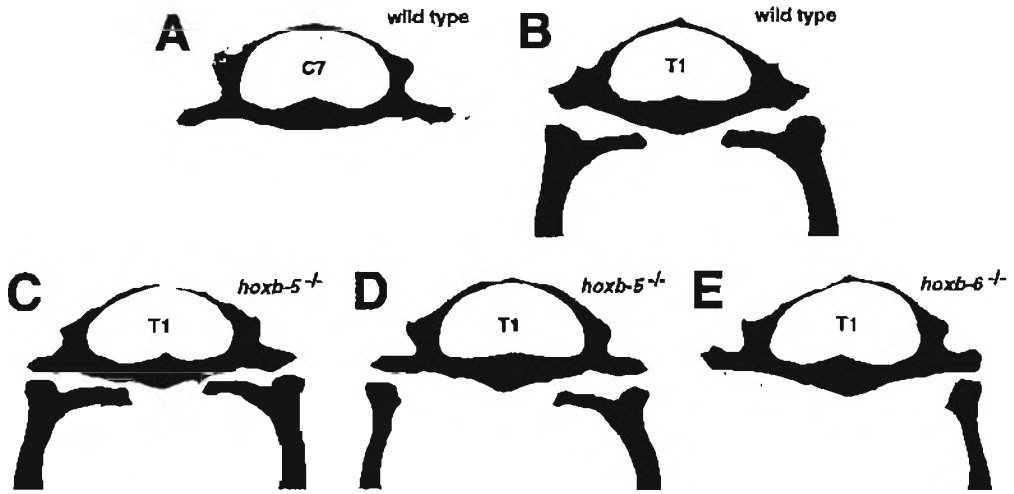

Figure 8. Linear progession of the T1 → C7 transformation in *hoxb-5*⁻ and *hoxb-6*⁻ mutants. Shown are rostral views of alizarin red-stained, adult vertebrae following dissection: wild-type seventh cervical (*A*, C7) and first thoracic vertebrae (*B*, T1), T1 vertebrae from two *hoxb-5*⁻ homozygotes (*C,D*), and one *hoxb-6*⁻ homozygote (*E*). Ribs were removed from T1 vertebrae to reveal the lateral processes of each vertebra. In wild-type adult vertebrae, the lateral processes of C7 lie at right angles to the vertebral body and thus are distinguishable from those of T1, where this sharp right angle does not exist. Homozygous mutants of *hoxb-5*⁻ (*D*) or *hoxb-6*⁻ (*E*) that display rib defects invariably have T1 vertebrae with processes resembling those of C7. In *D*, only the left rib head is missing and yet both lateral processes are similar to those of C7. In *E*, a rib is missing from the left side representing a complete T1 → C7 transformation on this side of the vertebra. (*C*) Even in animals showing no overt defect, the processes of the T1 vertebra appear to be altered towards those of C7.

The development of the axial skeleton in vertebrates occurs via a complex set of processes involving cell migration, cell differentiation, and cell–cell interactions (Verbout 1985; Christ and Whiting 1992; Balling et al. 1993). It is likely that a number of *Hox* genes, in addition to *hoxb-5* and *hoxb-6*, are involved in the specification of the lower cervical and upper thoracic region of the animal. Recently, the phenotypes of mice with disruptions in *hoxa-5* and *hoxa-6*, genes that are paralogs of *hoxb-5* and *hoxb-6*, respectively, have been reported (Jeannotte et al. 1993; Kostic and Capecchi 1994). Interestingly, both *hoxa-5*⁻ and *hoxa-6*⁻ homozygotes have ribs on C7. Therefore, mutations in *hoxa-5/hoxa-6* and in *hoxb-5/hoxb-6* have opposing consequences on the specification of the C7 → T1 transition region, the former giving rise to C7 vertebrae that resemble T1 (a posterior transformation) and the latter giving rise to T1 vertebrae that are similar to C7 (an anterior transformation). The opposite polarities exhibited by these genes in specifying the same vertebrae suggest that this transcriptional complex may have a built-in ability to make adjustments during development and thereby be sensitive to feedback circuitry that would mediate these adjustments. We anticipate that opposite polarities in the function of *Hox* genes participating in the formation of common structures will be found to be a recurring, rather than an isolated, theme.

One clue that adjustments can be made during development is the common observation that the consequences of gene disruptions can be unilateral or show more severe defects on one side of the mutant animal than on the other. The sidedness of the mutant defects appears to be random. This property is not specific to mutations in *hoxb-5* or *hoxb-6* but is observed in most, if not all, mice with *Hox* mutations. Furthermore, it has been observed in mice with targeted mutations in genes unrelated to the *Hox* genes. A particularly striking example is observed in *fgf-3*⁻ homozygotes (Mansour et al. 1993). These mice show severe defects in the formation of the inner ear. However, 80% of the mutant mice have one completely defective inner ear and one apparently functional inner ear. This variability in the expressivity of the mutation cannot be attributed to "leakage" of the mutation because the documentation that it is a null mutation is strong. Furthermore, variation in the genetic background cannot account for this variability in expressivity because the variability is observed within individual mutant animals. Rather, we must postulate that there is a gene, or genes, that is compensating for the mutation and that the utilization of compensatory circuits is different on one side of the mutant animal relative to the other. Compensation for mutations could be a stochastic process, or reflect an adjustment to the effects of the mutations. If the latter is true, it is unlikely that compensations during development would occur solely in response to a mutation but, rather, would reflect a process occurring during normal development.

Relation to human disorders

Unilateral defects are a common feature of several human congenital disorders, and it is interesting that several of the defects that we observe in *hoxb-5*⁻ and *hoxb-6*⁻ mutants are also observed in various syndromes seen

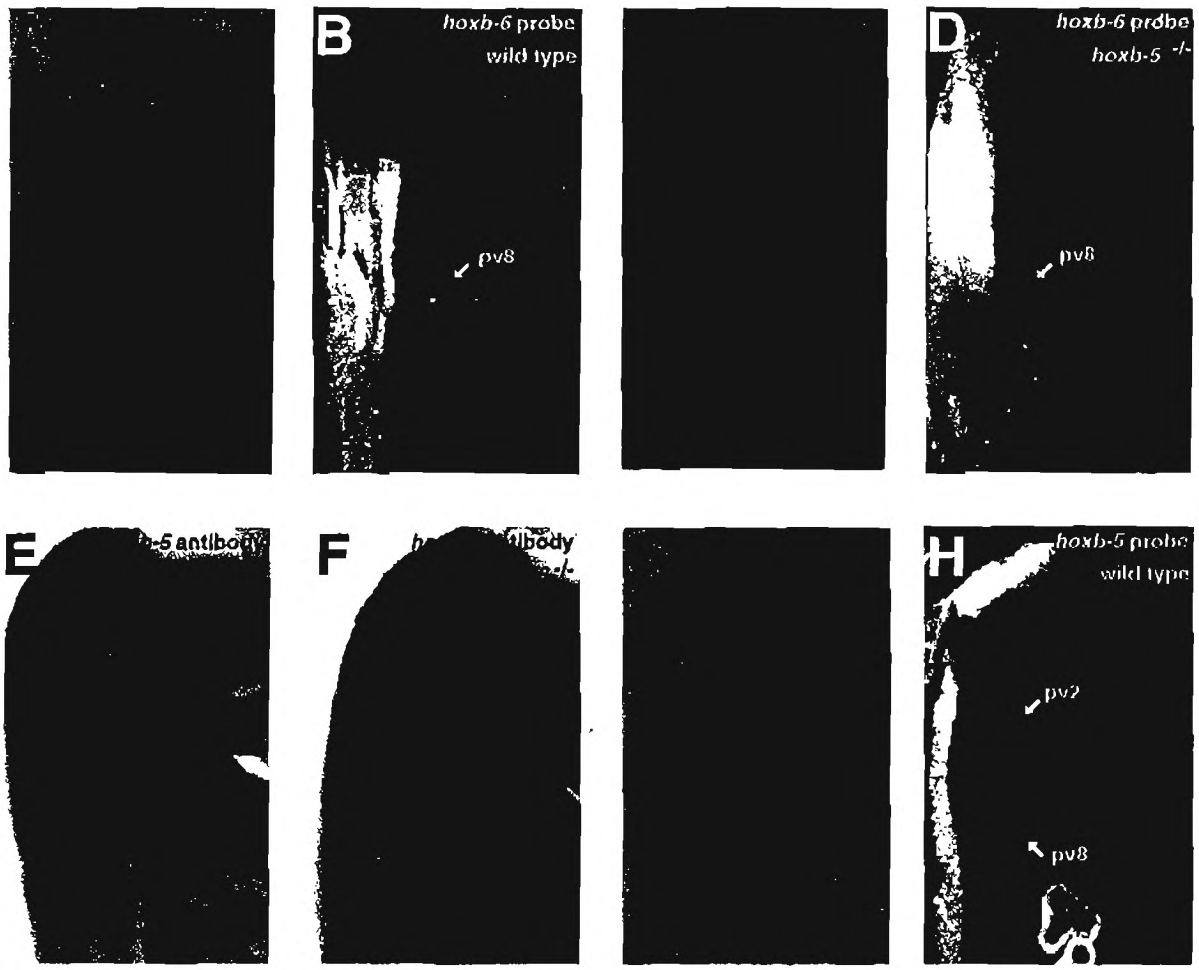

Figure 9. Expression of *hoxb-6* and *hoxb-5* in wild-type and in *hoxb-5*$^-$ and *hoxb-6*$^-$ mutant embryos. Parasagittal sections of E12.5 wild-type (*A,B,G,H*) and *hoxb-5*$^-$ homozygotes (*C,D*) were hybridized with [^{33}P]UTP-labeled *hoxb-6* (*A,B,C,D*) and *hoxb-5* (*G,H*) riboprobes, stained with hematoxylin after autoradiography and viewed with bright-field (*A,C,G*) and dark-field (*B,D,H*) illumination. The *hoxb-6* probe shows that the anterior expression boundary occurs at pv 8 in both wild-type (*A,B*), and homozygous *hoxb-5*$^-$ (*C,D*) embryos. The position of pv8 in these embryos was confirmed from its association in separate sections with the first rib primordium (not shown). (*E,F*) Hemisected wild-type and homozygous *hoxb-6*$^-$ E12.5 embryos were immunostained with anti-hoxb-5 antibody (Wall et al. 1992) and counterstained with alcian blue. No difference in *hoxb-5* expression was detected in wild-type and *hoxb-6*$^-$ embryos. The anterior boundary of protein expression (*top* arrow) occurs at pv2, whereas a posterior boundary is observed at pv8 (*bottom* arrow). (*G,H*) The anterior RNA expression boundary for *hoxb-5* also occurs at pv2 (*top* arrow), whereas no posterior boundary is observed at pv8 (*bottom* arrow).

in humans (McKusick 1992). For instance, unilateral bifid ribs have been observed in man. On the other hand, asymmetries in the lower cervical vertebrae have not been reported, partially because in humans, cervical vertebrae C3–C7 are indistinguishable, perhaps preventing the identification of potential homeotic transformations. Although the vertebral artery normally enters the foramen at C6, occasionally this position will shift down to C7. This can occur either uni- or bilaterally, but it is unknown whether there is a genetic component to this shifting (Bland and Boushey 1990).

The rostrally shifted shoulder phenotype that we observe in *hoxb-5*$^-$ homozygotes is similar in nature to that of the Sprengel anomaly observed in humans (McKusick 1992). As seen in humans, the scapula is located in a higher position, with its lower angle turned toward the spine. This can occur either unilaterally or bilaterally. However, in humans, the predominant form of Sprengel anomaly appears to be autosomal dominant, although a recessive form may also exist (Wilson et al. 1971). The Sprengel anomaly is frequently associated with Klippel–Feil syndrome and although we do not see evidence of Klippel–Feil-like cervical fusions in *hoxb-5*$^-$ homozygotes, it is interesting that we observe C2–C3 cervical fusions, similar to type II Klippel–Feil, when the *hoxb-5*$^-$ mutation is homozygous in a *hoxa-4*$^-$ homozygous background (D.E. Rancourt and M.R. Capecchi, unpubl.).

In summary, we have examined the phenotypic consequences of disrupting *hoxb-5* and *hoxb-6* in mice. *hoxb-5*$^-$ mutant mice show an anterior shift in the position of the forelimbs relative to the axial skeleton, arguing that *Hox* genes are components of the genetic program that specifies limb position in vertebrates, as well as of the programs that regulate the formation of the limb bones themselves. *hoxb-6*$^-$ homozygotes display defects in the formation of the first and second rib and the first intercostal nerve. Mutations in either *hoxb-5* or *hoxb-6* also cause anterior transformation of C6, C7, and T1. Unexpectedly, *hoxb-5* and *hoxb-6* transheterozygotes show the same anterior transformations, suggesting that the two genes interact to specify these cervicothoracic vertebrae. Nonallelic noncomplementation may provide a relatively simple test for identifying genetic interactions between *Hox* genes mediating the formation of common structures.

Materials and methods

Generation of hoxb-5$^-$ *and* hoxb-6$^-$ *mice*

Genomic clones surrounding the *hoxb-5* and *hoxb-6* genes were isolated from a C57Bl/6 genomic library using ^{32}P-labeled oligonucleotides specific for both sequences (Krumlauf et al. 1987; Schughart et al. 1988). The identity of each gene was confirmed by both restriction enzyme mapping and DNA sequence analysis. Individual targeting vectors for *hoxb-5* and *hoxb-6* were constructed by the insertion of genomic sequences encompassing each gene between HSV-1 and HSV-2 thymidine kinase genes (Chisaka and Capecchi 1991) and the insertion of *neo*^{r} into the first coding exon. pB5neo2TK (Fig. 1A) was derived from an 8.9-kb *Eco*RI genomic fragment in which the MC1neo poly(A) cassette (Thomas and Capecchi 1987) was inserted into the *Bam*HI site within the first exon (Krumlauf et al. 1987). Similarly, pB6neo2TK (Fig. 1A) was derived from a 10.1-kb *Bam*HI genomic fragment that contained an insertion of an RNA polymerase II/*neo*–poly(A) cassette (Deng et al. 1993) within the *Eco*RI site of the first exon.

Following linearization, gene targeting vectors were introduced into CC1.2 ES cells by electroporation. Targeted clones were enriched by positive–negative selection (Mansour et al. 1988) and identified by Southern analysis using hybridization probes that flanked the region of either targeting vector (Thomas and Capecchi 1987). The resulting cell lines, 2c6 and 3h12, were used to generate *hoxb-6*$^-$ and *hoxb-5*$^-$ mice, respectively, as described previously (Thomas and Capecchi 1990).

DNA analysis

Genomic DNAs were isolated from ES cells and animals by proteinase K digestion and phenol–chloroform extraction as described previously (Thomas and Capecchi 1987; Mansour and Capecchi 1993). Southern blot analysis was performed using BiotraceRP nylon (Gelman Scientific) membranes as recommended by the manufacturer. Probes were labeled with ^{32}P by random priming (Pharmacia). The *hoxb-6* flanking probe (Fig. 1F, probe A) is a 2.5-kb *Eco*RI–*Bam*HI fragment lying immediately 5′ to genomic sequences used in the *hoxb-6* gene targeting vector. The *hoxb-5* flanking probe (Fig. 1F, probe C) is a 0.9-kb *Hin*dIII–*Sau*3A fragment 3′ to the sequences used in the *hoxb-5* gene targeting vector. An internal probe (Fig. 1F, probe B) is a 1.5-kb *Bam*HI fragment that was used for genotypic analysis of mice.

Histology, in situ hybridization, and skeletal analysis

Newborn and adult mice were killed by CO_2 asphyxiation. Histological sections were collected and stained regressively with hematoxylin and eosin as described (Chisaka and Capecchi 1991). In situ hybridization to E12.5 embryo sections was performed as described previously using ^{33}P-labeled riboprobes (Carpenter et al. 1993). The *hoxb-6* probe was made from a 330-bp *Pvu*II–*Eco*RI fragment (Schughart et al. 1988) that was subcloned into *Sma*I–*Eco*RI sites of pBluescript SK. The *hoxb-5* probe was synthesized from a 450-bp *Bam*HI–*Hin*dIII cDNA fragment (Krumlauf et al. 1988) subcloned into pBluescript KS(+).

Skeletons of newborns were stained with alcian blue 8GX and alizarin red S as described previously (Mansour et al. 1993). Preparations of adult skeletons were similar, except that the carcasses were fixed in 4% formaldehyde and stained only with alizarin red S in 1% KOH (Kostic and Capecchi 1994).

Whole-mount histochemistry and immunohistochemistry

Mothers bearing mid-gestation embryos were killed by cervical dislocation, and conceptuses were dissected in phosphate-buffered saline (PBS). E12.5 embryos used for immunostaining with anti-hoxb-5 antisera were fixed 2 hr in Bouin's, hemisected, and bleached overnight with several changes of methanol/DMSO/30% H_2O_2 (4:1:1) (Wall et al. 1992). All other embryos were pinned (ventral side up) on 4-cm dissecting petri dishes (Carpenter et al. 1993) and fixed in 4% paraformaldehyde/PBS (2 hr); they were then rinsed in PBS and eviscerated following a ventral midline incision from the umbilical cord to the snout. Carcasses used for immunohistochemistry and lectin histochemistry were bleached in methanol/DMSO/30% H_2O_2 (4:1:1).

Whole-mount immunohistochemistry on hemisected E12.5 embryos using anti-hoxb-5 antisera was performed essentially as described by Wall et al. (1992), except that $NiCl_2$ was not included in the peroxidase staining reaction. Similarly, whole-mount neurofilament staining using the 2H3 anti-155-kD neurofilament monoclonal antibody (Dodd et al. 1988; Chisaka et al. 1992) was conducted using the method of Wall et al. (1992). Following peroxidase staining, embryos were preincubated in cartilage staining buffer (CSB: 70% methanol, 5% acetic acid) for 30 min and then stained with 0.01% alcian blue 8GX in CSB for 2 hr at room temperature. Stained carcasses were destained by rinsing thoroughly in CSB, followed by methanol, and cleared in benzoic acid, benzyl benzoate (1:2).

For lectin histochemistry, carcasses were bleached as described above and stained with horseradish peroxidase (HRP)-conjugated peanut agglutinin (U.S. Biochemical) at 100 μg/ml using methods identical to those for immunohistochemistry (above). After HRP staining, carcasses were taken through a methanol series to 100% methanol and cleared as above.

Dye injections were performed essentially as described previously (Carpenter et al. 1993) except that alternating injections of fluorescent carbocyanine dyes (DiI and DiO) were limited to the cervical nerves.

Acknowledgments

We thank M. Allen, S. Barnett, C. Lenz, E. Nakashima, and S. Tamowski for technical assistance. We are grateful to B. Hogan and the Developmental Studies Hybridoma Bank for providing

us with hoxb-5 and 2H3–155-kd neurofilament antibody, respectively. Dr. E. Carpenter helped with the injection of carbocyanine dyes, and L. Oswald helped with the preparation of the manuscript. D.E.R. was funded by fellowships from the Medical Research Council of Canada and the AMGEN Corporation.

The publication costs of this article were defrayed in part by payment of page charges. This article must therefore be hereby marked "advertisement" in accordance with 18 USC section 1734 solely to indicate this fact.

References

Akam, M.E. 1987. The molecular basis for metameric pattern in the *Drosophila* embryo. *Development* **101**: 1–22.

Balling, R., C. Ebensperger, I. Hoffmann, K. Imai, H. Koseki, Y. Mizutani, and J. Wallin. 1993. The genetics of skeletal development. *Ann. Genet.* **36**: 56–62.

Bland, J.H. and D.R. Boushey. 1990. Anatomy and physiology of the cervical spine. *Semin. Arthritis Rheum.* **20**: 1–20.

Braun, T., M.A. Rudnicki, H.-H. Arnold, and R. Jaenisch. 1992. Targeted inactivation of the muscle regulatory gene *Myf-5* results in abnormal rib development and perinatal death. *Cell* **71**: 369–382.

Capecchi, M.R. 1989. Altering the genome by homologous recombination. *Science* **244**: 1288–1292.

———. 1994. Targeted gene replacement. *Sci. Am.* **270**: 54–61.

Carpenter, E.M., J.M. Goddard, O. Chisaka, N.R. Manley, and M.R. Capecchi. 1993. Loss of *Hox-A1* (*Hox-1.6*) function results in the reorganization of the murine hindbrain. *Development* **118**: 1063–1075.

Chen, J.M. 1952. Studies on the morphogenesis of the mouse sternum II. Experiments on the origin of the sternum and its capacity for self-differentiation in vitro. *J. Anat.* **86**: 387–401.

———. 1953. Studies on the morphogenesis of the mouse sternum. III. Experiments on the closure and segmentation of the sternal bands. *J. Anat.* **87**: 130–149.

Chevalier, A., M. Kieny, A. Mauger, and P. Sengel. 1977. Developmental fate of the somitic mesoderm in the chick embryo. In *Vertebrate limb and somite morphogenesis* (ed. D.A. Ede, J.R. Hinchliffe, and M. Balls), pp. 421–432. Cambridge University Press, Cambridge, UK.

Chisaka, O. and M.R. Capecchi. 1991. Regionally restricted developmental defects resulting from targeted disruption of the mouse homeobox gene *Hox-1.5*. *Nature* **350**: 473–479.

Chisaka, O., T.S. Musci, and M.R. Capecchi. 1992. Developmental defects of the ear, cranial nerves and hindbrain resulting from targeted disruption of the mouse homeobox gene *Hox-1.6*. *Nature* **355**: 516–520.

Christ, B. and J. Whiting. 1992. From somites to vertebral column. *Ann. Anat.* **174**: 23–32.

Condie, B.G. and M.R. Capecchi. 1993. Mice homozygous for a targeted disruption of *Hoxd-3* (*Hox-4.1*) exhibit anterior transformations of the first and second cervical vertebrae, the atlas and the axis. *Development* **119**: 579–595.

———. 1994. Mice with targeted disruptions in the paralogous genes *hoxa-3* and *hoxd-3* reveal synergistic interactions. *Nature* **370**: 304–307.

Davis, A.P. and M.R. Capecchi. 1994. Axial homeosis and appendicular skeleton defects in mice with a targeted disruption of *hoxd-11*. *Development* **120**: 2187–2198.

Deng, C., K.R. Thomas, and M.R. Capecchi. 1993. Location of crossovers during gene targeting with insertion and replacement vectors. *Mol. Cell. Biol.* **13**: 2134–2140.

Dodd, J., S.B. Morton, D. Karagogeos, M. Yamamoto, and T.M. Jessell. 1988. Spatial regulation of axonal glycoprotein expression on subsets of embryonic spinal neurons. *Neuron* **1**: 105–116.

Dollé, P., A. Dierich, M. LeMeur, T. Schimmang, B. Schuhbaur, P. Chambon, and D. Duboule. 1993. Disruption of the *Hoxd-13* gene induces localized heterochrony leading to mice with neotenic limbs. *Cell* **75**: 431–441.

Duboule, D. and P. Dollé. 1989. The structural and functional organization of the murine *Hox* gene family resembles that of *Drosophila* homeotic genes. *EMBO J* **8**: 1497–1505.

Eid, R., H. Koseki, and K. Schughart. 1993. Analysis of lacZ reporter genes in transgenic embryos suggests the presence of several cis-acting regulatory elements in the murine *hoxb-6* gene. *Dev. Dyn.* **196**: 205–216.

Garcia-Fernández, J. and P.W.H. Holland. 1994. Archetypal organization of the amphioxus *Hox* gene cluster. *Nature* **370**: 563–566.

Gaunt, S.J., P.L. Coletta, D. Pravtcheva, and P.T. Sharpe. 1990. Mouse Hox-3.4: Homeobox sequence and embryonic expression patterns compared with other members of the Hox gene network. *Development* **109**: 329–339.

Gendron-Maguire, M., M. Mallo, M. Zhang, and T. Gridley. 1993. *Hoxa-2* mutant mice exhibit homeotic transformation of skeletal elements derived from cranial neural crest. *Cell* **75**: 1317–1331.

Götz, W., G. Fischer, and R. Herken. 1991. Lectin binding pattern in the embryonal and early fetal human vertebral column. *Anat. Embryol.* **184**: 345–353.

Graham, A., N. Papalopulu, and R. Krumlauf. 1989. The murine and *Drosophila* homeobox gene complexes have common features of organization and expression. *Cell* **57**: 367–378.

Hays, T.S., R. Duering, B. Robertson, M. Prout, and M.T. Fuller. 1989. Interacting proteins identified by genetic interactions: A missense mutation in α-tubulin fails to complement alleles of the testis-specific β-tubulin gene of *Drosophila melanogaster*. *Mol. Cell. Biol.* **9**: 875–884.

Heitman, J., N.R. Movva, and M.N. Hall. 1991. Targets for cell cycle arrest by the immunosuppressant rapamycin in yeast. *Science* **253**: 905–909.

Holland, P.W.H. and B.L.M. Hogan. 1988. Spatially restricted pattern of expression of the homeobox-containing gene, *Hox-2.1* during mouse embryogenesis. *Development* **102**: 159–174.

Holland, P.W.H., L.Z. Holland, N.A. Williams, and N.D. Holland. 1992. An amphioxus homeobox gene: Sequence conservation, spatial expression during development and insights into vertebrate evolution. *Development* **116**: 653–661.

Hunt, P., M. Gulisano, M. Cook, M.-H. Sham, A. Faiella, D. Wilkinson, E. Boncinelli, and R. Krumlauf. 1991. A distinct *Hox* code for the branchial region of the vertebrate head. *Nature* **353**: 861–864.

Jeannotte, L., M. Lemieux, J. Charron, F. Poirier, and E.J. Robertson. 1993. Specification of axial identity in the mouse: Role of the *Hoxa-5* (*Hox-1.3*) gene. *Genes & Dev.* **7**: 2085–2096.

Kappen, C., K. Schughart, and F.H. Ruddle. 1989. Two steps in the evolution of *Antennapedia*-class vertebrate homeobox genes. *Proc. Natl. Acad. Sci.* **86**: 5459–5463.

Kissinger, C.R., B. Liu, E. Martin-Blanco, T.B. Kornberg, and C.O. Pabo. 1990. Crystal structure of an engrailed homeodomain-DNA complex at 2.8 Å resolution: A framework for understanding homeodomain-DNA interactions. *Cell* **63**: 579–590.

Kostic, D. and M.R. Capecchi. 1994. Targeted disruptions of the murine *hoxa-4* and *hoxa-6* genes result in homeotic trans-

formations of components of the vertebral column. *Mech. Dev.* 46: 231–247.

Krumlauf, R., P.W. Holland, J.H. McVey, and B.L.M. Hogan. 1987. Developmental and spatial patterns of expression in the mouse homeobox gene *Hox 2.1*. *Development* 99: 603–617.

Kuratani, S.C. and N.A. Wall. 1992. Expression of Hox 2.1 protein in restricted populations of neural crest cells and pharyngeal ectoderm. *Dev. Dyn.* 195: 15–28.

LeMouellic, H., Y. Lallemand, and P. Brulet. 1992. Homeosis in the mouse induced by a null mutation in the *Hox-3.1* gene. *Cell* 69: 251–264.

Lewis, E.B. 1978. A gene complex controlling segmentation in *Drosophila*. *Nature* 276: 565–570.

Lufkin, T., A. Dierich, M. LeMeur, M. Mark, and P. Chambon. 1991. Disruption of the *Hox-1.6* homeobox gene results in defects in a region corresponding to its rostral domain of expression. *Cell* 66: 1105–1119.

Mansour, S.L., K.R. Thomas, and M.R. Capecchi. 1988. Disruption of the proto-oncogene *int-2* in mouse embryo-derived stem cells: A general strategy for targeting mutations to nonselectable genes. *Nature* 336: 348–352.

Mansour, S.L., J.M. Goddard, and M.R. Capecchi. 1993. Mice homozygous for a targeted disruption of the proto-oncogene *int-2* have developmental defects in the tail and inner ear. *Development* 117: 13–28.

Mark, M., T. Lufkin, J.L. Vonesch, E. Ruberte, J.-C. Olivo, P. Dollé, P. Gorry, A. Lumsden, and P. Chambon. 1993. Two rhombomeres are altered in *Hoxa-1* mutant mice. *Development* 119: 319–338.

McKusick, V.A. 1992. *Mendelian inheritance in man: Catalogs of autosomal dominant, autosomal recessive, and X-linked phenotypes*. Johns Hopkins University Press, Baltimore, MD.

Otting, G., Y.Q. Qian, M. Billeter, M. Muller, M. Affolter, W.J. Gehring, and K. Wuthrich. 1990. Protein–DNA contacts in the structure of a homeodomain–DNA complex determined by nuclear magnetic resonance spectroscopy in solution. *EMBO J.* 9: 3085–3092.

Ramirez-Solis, R., H. Zheng, J. Whiting, R. Krumlauf, and A. Bradley. 1993. *Hoxb-4* (*Hox-2.6*) mutant mice show homeotic transformation of a cervical vertebra and defects in the closure of the sternal rudiments. *Cell* 73: 279–294.

Rijli, F.M., M. Mark, S. Lakkaraju, A. Dierich, P. Dollé, and P. Chambon. 1993. A homeotic transformation is generated in the rostral branchial region of the head by disruption of *Hoxa-2*, which acts as a selector gene. *Cell* 75: 1333–1349.

Rine, J. and I. Herskowitz. 1987. Four genes responsible for a position affect on expression from HML and HMR in Saccharomyces cerevisiae. *Genetics* 116: 9–22.

Schughart, K., M.F. Utset, A. Awgulewitsch, and F.H. Ruddle. 1988. Structure and expression of Hox-2.2, a murine homeobox-containing gene. *Proc. Natl. Acad. Sci.* 85: 5582–5586.

Schughart, K., C.J. Bieberich, R. Eid, and F.H. Ruddle. 1991. A regulatory region from the mouse *Hox-2.2* promoter directs gene expression into developing limbs. *Development* 112: 807–811.

Scott, M.P. 1992. Vertebrate homeobox gene nomenclature. *Cell* 71: 551–553.

Shen, W., K. Detmer, T.A. Simonitch-Eason, H.J. Lawrence, and C. Largman. 1991. Alternative splicing of the HOX 2.2 homeobox gene in human hematopoietic cells and murine embryonic and adult tissues. *Nucleic Acids Res.* 19: 539–545.

Small, K.M. and S.S. Potter. 1993. Homeotic transformations and limb defects in *Hoxa-11* mutant mice. *Genes & Dev.* 7: 2318–2328.

Steams, T. and D. Botstein. 1988. Unlinked noncomplementation: Isolation of new conditional-lethal mutations in each of the tubulin genes of Saccharomyces cerevisiae. *Genetics* 119: 249–260.

Thomas, K.R. and M.R. Capecchi. 1987. Site-directed mutagenesis by gene targeting in mouse embryo-derived stem cells. *Cell* 51: 503–512.

———. 1990. Targeted disruption of the murine *int-1* proto-oncogene resulting in severe abnormalities in midbrain and cerebellar development. *Nature* 346: 847–850.

Varkey, J.P., P.L. Jansma, A.N. Minniti, and S. Ward. 1993. The Caenorhabditis elegans *spe-6* gene is required for major sperm protein assembly and shows second site non-complementation with an unlinked deficiency. *Genetics* 133: 79–86.

Verbout, A.J. 1985. The development of the vertebral column. *Adv. Anat. Embryol. Cell Biol.* 90: 1–122.

Wall, N.A., C.M. Jones, B.L.M. Hogan, and C.V.E. Wright. 1992. Expression and modification of *hox-2.1* protein in mouse embryos. *Mech. Dev.* 37: 111–120.

Wilson, M.G., V.G. Miksity, and N.W. Shinno. 1971. Dominant inheritance of Sprengel's deformity. *J. Pediatr.* 79: 818–821.

Zappavigna, V., D. Sartori, and F. Mavilio. 1994. Specificity of HOX protein function depends on DNA–protein and protein–protein interactions, both mediated by the homeo domain. *Genes & Dev.* 8: 732–744.